Surface Characterization of CeO_2/SiO_2 and $V_2O_5/CeO_2/SiO_2$ Catalysts by Raman, XPS, and Other Techniques

Benjaram M. Reddy* and Ataullah Khan

Inorganic and Physical Chemistry Division, Indian Institute of Chemical Technology, Hyderabad 500 007, India

Yusuke Yamada and Tetsuhiko Kobayashi

National Institute of Advanced Industrial Science and Technology (AIST), 1-8-31 Midorigaoka, Ikeda, Osaka 563-8577, Japan

Stéphane Loridant and Jean-Claude Volta

Institut de Recherches sur la Catalyze, CNRS, 2 Avenue A. Einstein, 69626 Villeurbanne Cedex, France

Received: May 13, 2002; In Final Form: July 31, 2002

X-ray diffraction, Raman, and X-ray photoelectron spectroscopy were utilized to characterize CeO_2/SiO_2 supports and $V_2O_5/CeO_2/SiO_2$ catalysts calcined at different temperatures from 773 to 1073 K. The CeO_2/SiO_2 support was obtained by an aqueous deposition precipitation method, and vanadium oxide was applied to the calcined support (773 K) by using a wet impregnation technique. The XRD and Raman results suggest that the CeO_2/SiO_2 carrier is thermally quite stable up to 1073 K calcination temperature and primarily consists of a CeO_2 overlayer on the SiO_2 substrate. The CeO_2/SiO_2 support also accommodates a layer of vanadia in a highly dispersed state on its surface. In particular, no crystalline V_2O_5 was observed. The O 1s, Si 2p, Ce 3d, and V 2p core level photoelectron peaks of CeO_2/SiO_2 and $V_2O_5/CeO_2/SiO_2$ are sensitive to the calcination temperature. The XPS line shapes and the corresponding binding energies indicate that the dispersed vanadium oxide interacts selectively with the ceria portion of the CeO_2/SiO_2 carrier and readily forms $CeVO_4$. The XRD and Raman techniques, in particular, provide direct evidence about the formation of $CeVO_4$. The V/Ce and V/Si atomic ratios, as determined by XPS measurements, reveal that vanadia is mainly confined to ceria at all calcination temperatures. No significant changes in the oxidation states of V(V) and Si(IV) are noted with increasing calcination temperature. However, in the case of cerium oxide stabilization of Ce(III) was observed at higher calcination temperatures.

Introduction

Among the rare earth metal oxides that have been widely investigated in ceramics and industrial catalysis, cerium dioxide (CeO_2) certainly stands apart.[1,2] Ceria is one of the most important components of fluid catalytic cracking (FCC) catalysts and three-way catalysts (TWC).[3] Other significant applications of cerium-containing catalysts include removal of soot from diesel engine exhaust,[4] removal of organics from wastewaters,[5] as an additive for combustion catalysts,[6] and in fuel cell processes.[7] The influence of cerium-containing materials in various other catalytic processes is being actively investigated.

Ceria forms part of TWC formulations because it acts as an oxygen buffer by storing and releasing oxygen under controlled conditions.[1,8] The Ce^{4+}/Ce^{3+} redox couple present in ceria-containing catalysts is known to be responsible for this intrinsic property. In general, the TWCs are required to possess high thermal stability and mechanical strength, as they are located close to the engine. It is an established fact in the literature that pure ceria alone is poorly thermostable.[9,10] It easily gets deactivated due to sintering at higher temperatures, thereby loosing its oxygen storage capacity (OSC). The loss in surface area is usually related to changes in the pore structure and to crystallite growth. It is therefore essential to improve its textural stability. Recent studies have suggested that formation of mixed oxides of ceria with cations such as Zr^{4+}, Al^{3+}, and La^{3+} (see refs 11−14) enhances the catalytic,[15,16] textural,[17] redox,[18,19] and oxygen storage properties[18−21] of ceria and the so-formed mixed oxides also exhibit good thermal stability. Silica is a well-known support, which exhibits good chemical resistance, thermal stability, and high specific surface area. However, investigations on ceria−silica combination oxides are scarce in the literature.[22,23]

Supported V_2O_5 is the basic component of industrial catalysts for selective oxidation and ammoxidation of various hydrocarbons.[24−34] Moreover, vanadium oxide containing catalysts are among the best for the reduction of NO_x with NH_3, which is an important process for the purification of exhaust gases from power plants (SCR).[28] Oxidation catalysts are receiving a great deal of attention because of their major role both in the production of materials required and in the destruction of undesired products by total catalytic oxidation. As a consequence, considerable attention has been focused on the preparation, characterization, and evaluation of vanadium oxide catalysts deposited on various single oxides (Al_2O_3, SiO_2, TiO_2, ZrO_2, and CeO_2) as well as on mixed oxides (TiO_2-SiO_2, TiO_2-ZrO_2, and $TiO_2-Al_2O_3$).[24−40] The present study was undertaken to make a $V_2O_5/CeO_2/SiO_2$ combination catalyst

10.1021/jp021195v CCC: $22.00
Published on Web 10/01/2002

where ceria acts as a promoter and silica forms part of the support. The above discussion indicates that combination of vanadia (known for its redox properties) and ceria (known for its oxygen storage and release functions) may give rise to a better catalytic system that may catalyze extraneous redox reactions for both selective and nonselective oxidations, the latter having enormous applications in the field of environmental catalysis for the oxidative removal of volatile organic compounds and other noxious emissions.

In this study, the CeO_2/SiO_2 combination carrier was prepared by a deposition precipitation method and was impregnated with vanadium pentoxide. The obtained CeO_2/SiO_2 carrier and the $V_2O_5/CeO_2/SiO_2$ catalyst were subjected to thermal treatments from 773 to 1073 K to determine the thermal stability, the dispersion of vanadium oxide, and the physicochemical properties of these materials. These effects have been investigated by means of XRD, Raman, XPS, and other techniques.

Experimental Section

Catalyst Preparation. The CeO_2/SiO_2 mixed oxide (1:1 mole ratio based on oxides) was prepared by a deposition precipitation method. In a typical experiment, the requisite quantities of cerium ammonium nitrate (Loba Chemie, GR grade), dissolved separately in deionized water, and colloidal silica (40 wt %, Fluka, AR grade) were mixed together. Dilute aqueous ammonia solution was added dropwise to the above mixture solution with vigorous stirring until the precipitation was complete (pH = 8). The resulting product was filtered off, washed with deionized water, oven dried at 383 K for 12 h, and then calcined at 773 K for 5 h in air. Portions of this calcined support were once again heated at 873, 973, and 1073 K for 5 h in a closed electrical furnace in air. The rate of heating as well as of cooling was always maintained at 10 K/min.

The $V_2O_5/CeO_2/SiO_2$ catalysts were prepared by a standard wet impregnation method. To impregnate vanadium oxide (5 and 10 wt % V_2O_5) over the support, the requisite quantity of ammonium metavanadate (Fluka, AR grade) was dissolved in aqueous oxalic acid solution (1 M). To this clear solution, the finely powdered calcined (773 K) mixed oxide support was added. The excess water was then evaporated on a water bath with constant stirring, and the resulting material was oven dried at 393 K for 12 h and subsequently calcined at 773 K for 5 h in a closed muffle furnace in flowing oxygen. Portions of the finished catalysts were once again heated at 873, 973, and 1073 K for 5 h in air.

X-ray Diffraction. X-ray powder diffraction patterns have been recorded on a Siemens D500 diffractometer using Ni-filtered Cu Kα (0.15418 nm) radiation and standard recording conditions. The XRD phases present in the samples were identified with the help of the Powder Diffraction File-International Centre for Diffraction Data (PDF-ICDD). The average crystallite size of CeO_2 was estimated with the help of the Debye−Scherrer equation using the XRD data of all prominent lines.[41]

Raman Spectra. The Raman spectra were recorded at ambient temperature on a DILOR XY spectrometer equipped with a CCD detector. The emission line at 514.5 nm from an Ar^+ ion laser (Spectra Physics) was focused on the samples under the microscope so that the size of the analyzed spot was about 1 μm. The power of the incident beam on the sample was 3 mW. The time of acquisition was adjusted according to the intensity of the Raman scattering. The wavenumber values obtained from the spectra are accurate to within 2 cm^{-1}.

X-ray Photoelectron Spectroscopy. The XPS measurements were made on a Shimadzu (ESCA 3400) spectrometer by using Mg Kα (1253.6 eV) radiation as the excitation source. Charging of catalyst samples was corrected by setting the binding energy of adventitious carbon (C 1s) at 284.6 eV.[42,43] The finely ground oven-dried samples were dusted on a double stick graphite sheet and mounted on the standard sample holder. The sample holder was then transferred to the analysis chamber, which can house 10 samples at a time, through a rod attached to it. The XPS analysis was done at room temperature and pressures typically below 10^{-6} Pa. The samples were outgassed in a vacuum oven overnight before XPS measurements. Quantitative analysis of atomic ratios was accomplished by determining the elemental peak areas, following a Shirley background subtraction by the usual procedures documented in the literature.[42,43]

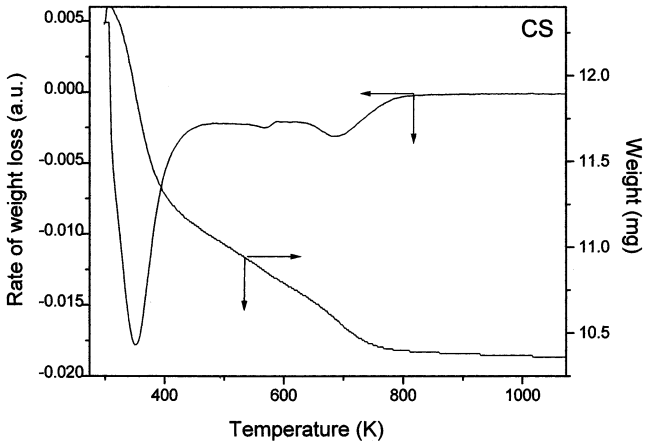

Figure 1. TGA and DTA profile of CeO_2/SiO_2 sample before calcination.

Thermal Analysis. The DTA-TGA curves were obtained on a Mettler Toledo TG-SDTA apparatus. The sample was heated from ambient temperature to 1173 K under nitrogen flow. The sample weight was ca. 12 mg, and the heating rate was 10 K/min.

BET Surface Area. The specific surface area of the samples was determined on a Micromeritics Gemini 2360 Instrument with N_2 physisorption at liquid N_2 temperature. Before measurements, the samples were oven dried at 393 K for 12 h and flushed in situ with He gas for 2 h.

Results and Discussion

The CeO_2/SiO_2 mixed oxide was subjected to TGA-DTA analysis before calcination. The thermogram, obtained between 273 and 1173 K and at a ramp of 10 K/min, is shown in Figure 1. As can be noted from this figure, this ceria−silica mixed oxide exhibits one major and two minor weight loss peaks. The major low-temperature peak in the range 309−463 K is primarily due to the loss of nondissociative adsorbed water as well as water held on the surface by hydrogen bonding. The minor weight loss peak in the 550−584 K range could be due to loss of water held in the micropores of the mixed oxide gel. A further loss of water occurs around 633−723 K due to dehydroxylation of the surface. The loss of weight from ambient to 470 K is about 10% and from 470 to 723 K is 5%. However, the weight loss between 723 and 1073 K is only about 1%. Thus over the temperature range between 723 and 1073 K, the CeO_2/SiO_2 mixed oxide is quite stable in terms of chemical composition for further impregnation by vanadia.

The calcined (773 K) CeO_2/SiO_2 carrier exhibited a N_2 BET surface area of 147 $m^2\ g^{-1}$. The theoretical quantity of V_2O_5 required to cover the support surface as a monomolecular layer can be estimated from the area occupied per $VO_{2.5}$ unit of the

TABLE 1: BET Surface Areas and Crystallite Size Measurements (CeO_2) of CeO_2/SiO_2 and $V_2O_5/CeO_2/SiO_2$ Samples Calcined at Different Temperatures

sample	BET SA ($m^2\ g^{-1}$ cat)	CeO_2 crystallite size (nm)
	773 K	
CeO_2/SiO_2	147	3.2
5% $V_2O_5/CeO_2/SiO_2$	96	3.5
10% $V_2O_5/CeO_2/SiO_2$	78	3.8
	873 K	
CeO_2/SiO_2	104	3.6
5% $V_2O_5/CeO_2/SiO_2$	72	5.0
10% $V_2O_5/CeO_2/SiO_2$	40	7.6
	973 K	
CeO_2/SiO_2	75	4.4
5% $V_2O_5/CeO_2/SiO_2$	38	12.6
10% $V_2O_5/CeO_2/SiO_2$	32	13.9
	1073 K	
CeO_2/SiO_2	54	6.0
5% $V_2O_5/CeO_2/SiO_2$	23	19.0
10% $V_2O_5/CeO_2/SiO_2$	17	20.6

bulk V_2O_5 (0.105 nm^2).[29] This estimate gives an amount of 0.145 wt % per m^2 of the support to cover its surface with a compact single layer of vanadium pentoxide structure.[26] However, the maximum quantity of vanadium oxide that can be formed as a monolayer depends not only on the specific surface area of the support material but also on the concentration of reactive surface hydroxyl groups. Therefore, the experimentally determined actual monolayer loading on various supports was always less than the theoretical estimation and corresponds to about 70% of the theoretical value.[26] In view of these reasons, nominal 5 and 10 wt % V_2O_5 loadings were selected in the present investigation to impregnate on the surface of the CeO_2/SiO_2 carrier. The specific surface areas of CeO_2/SiO_2 and $V_2O_5/CeO_2/SiO_2$ samples calcined at different temperatures are presented in Table 1. As seen from Table 1, the BET surface area of CeO_2/SiO_2 support decreased after calcination at higher temperatures due to sintering. A large decrease in the surface area of the CeO_2/SiO_2 carrier can be observed after impregnating with vanadium pentoxide. This could be due to the penetration of the dispersed vanadium oxide into the pores of the support, thereby narrowing its pore diameter and blocking some of the micropores.[26,44,45] Additionally, solid-state reactions between the dispersed vanadium oxide and the support may also contribute to the observed decrease in the BET surface areas, especially at higher calcination temperatures. The XRD and Raman measurements described in the subsequent paragraphs strongly support the latter possibility. However, an important point to be noted from the BET surface area measurements (Table 1) is that the decrease in the specific surface area is larger for vanadia-impregnated samples than for the pure support. In other words the pure ceria−silica mixed oxide is more thermally stable than vanadia-impregnated samples.

The X-ray powder diffraction patterns of the CeO_2/SiO_2 mixed oxide calcined at different temperatures is shown in Figure 2. As can be noted from this figure, the ceria/silica mixed oxide calcined at 773 K exhibits poor crystallinity. Only the broad diffraction lines due to CeO_2 (PDF-ICDD 34-0394) are visible. With increasing calcination temperature from 773 to 1073 K, a gradual increase in the intensity of the lines due to crystallization of cerium oxide is noted. The crystallite size of CeO_2 estimated from XRD measurements and presented in Table 1 supports this observation. The silica features are not observed from the XRD measurements, as it is known that silica is in the amorphous form even up to 1273 K calcination

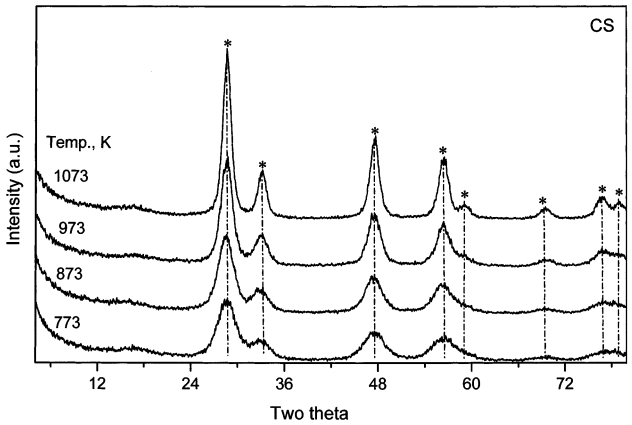

Figure 2. X-ray powder diffraction patterns of CeO_2/SiO_2 calcined at different temperatures: (*) lines due to CeO_2.

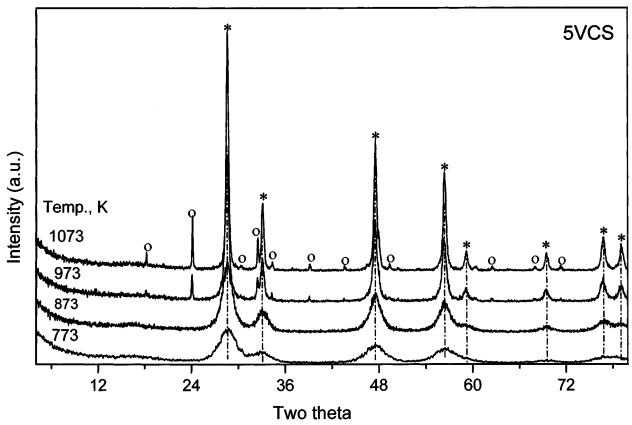

Figure 3. X-ray powder diffraction patterns of 5 wt % $V_2O_5/CeO_2/SiO_2$ calcined at different temperatures: (*) lines due to CeO_2; (○) lines due to $CeVO_4$.

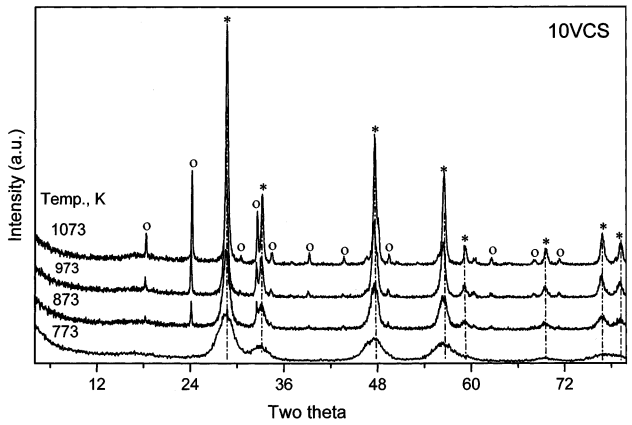

Figure 4. X-ray powder diffraction patterns of 10 wt % $V_2O_5/CeO_2/SiO_2$ calcined at different temperatures: (*) lines due to CeO_2; (○) lines due to $CeVO_4$.

temperature.[26,44] Another interesting observation to be noted from the XRD measurements is that ceria and silica do not form any compounds or mixed phases, as observed for ceria−zirconia and ceria−titania mixed oxides.[16−19,46,47]

The XRD patterns of the 5%$V_2O_5/CeO_2/SiO_2$ and 10% $V_2O_5/CeO_2/SiO_2$ samples calcined at different temperatures are shown in Figures 3 and 4, respectively. The XRD patterns of the 5% $V_2O_5/CeO_2/SiO_2$ sample (Figure 3) calcined at 773−873 K show only the broad diffraction lines due to CeO_2. As crystalline vanadia features are not apparent, it can be inferred that vanadium oxide is in a highly dispersed or amorphous form on

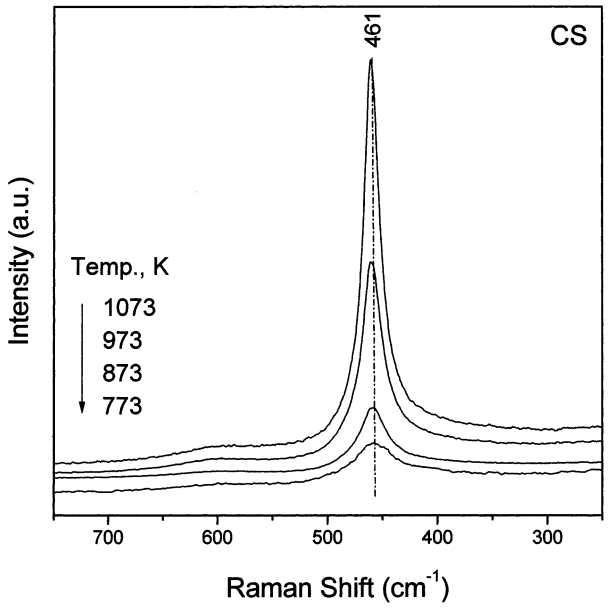

Figure 5. Laser Raman spectra of CeO_2/SiO_2 calcined at different temperatures.

the surface of the support. However, at 973 K in addition to the sharp CeO_2 lines, new lines with less intensity can be seen at $2\theta = 18.5$, 24, and 32.5, respectively. These lines are attributed to the formation of $CeVO_4$ (PDF-ICDD 12-0757). The intensity of these lines increases with increasing calcination temperature. In the case of the 10% $V_2O_5/CeO_2/SiO_2$ sample (Figure 4), the presence of XRD lines due to $CeVO_4$ can be seen even at the calcination temperature of 873 K, along with sharp diffraction lines due to CeO_2 oxide. With an increase of calcination temperature from 873 to 1073 K, a further increase in the intensity of the lines due to both CeO_2 and $CeVO_4$ is observed. Here too, XRD lines due to crystalline SiO_2 or compounds thereof are not observed irrespective of the calcination temperature. The preferential formation of $CeVO_4$ oxide indicates that vanadium oxide selectively interacts with the ceria portion of the ceria−silica carrier and forms this stable compound.

The influence of temperature on the crystallite size of ceria in various samples, as determined from X-ray line broadening, is shown in Table 1. The crystallite size of CeO_2 in CeO_2/SiO_2 samples increased from 3.2 to 6.0 nm with increasing calcination temperature from 773 to 1073 K, respectively. An interesting observation to be noted from Table 1 is that the impregnated vanadia appears to increase the crystallite size of CeO_2 in $V_2O_5/CeO_2/SiO_2$ samples after calcination at higher temperatures. Increasing vanadia loading also seems to increase the size of CeO_2 crystallites. These results suggest that the impregnated vanadia accelerates the grain growth of ceria. It is an interesting observation from this study.

Raman spectroscopy (RS) is a good technique for the elucidation of structures of complex transition metal oxides present either as bulk phases or as two-dimensional supported phases because RS directly probes structures and bonds by their vibrational spectrum. Therefore, this technique has been successfully used to discriminate between different structures on oxide surfaces.[48] As presented in Figure 5, the Raman spectrum of CeO_2/SiO_2 calcined at 773 K shows a prominent peak at about 457 cm^{-1} and a weak band at 600 cm^{-1}. The band at around 457 cm^{-1} corresponds with the triply degenerate F_{2g} mode and can be viewed as a symmetric breathing mode of the oxygen atoms around cerium ions.[49] With increasing calcination temperature from 773 to 1073 K, the band at ∼457 cm^{-1} shifts to ∼461 cm^{-1}, sharpens, and becomes more symmetrical. This could be due to better crystallization of ceria at higher calcination temperatures, as observed from XRD measurements. It is a known fact in the literature that the intensity of a Raman band depends on several factors including the grain size and morphology. In general, inhomogeneous strain and phonon confinement are responsible for the broad and asymmetric character of the bands as the particle size gets smaller at lower calcination temperatures.[50] The weak band observed near 600 cm^{-1} could correspond to a doubly degenerate LO mode of CeO_2.[49,51] Normally, this mode should not be observed by Raman spectroscopy but the presence of some defects can lead to a relaxation of the selection rules. In particular, this band has been linked to oxygen vacancies in the CeO_2 lattice.[52] This peak was observed in the case of all nanocrystallized samples, and its relative intensity increased as the particle size decreased.[49] The same phenomenon is apparent in the present study. For each sample, the spectra were recorded at several points and no shift in the band position or difference of width was noted. This observation reveals clearly that the CeO_2/SiO_2 sample is homogeneous. Silica did not show any Raman features, as reported in the literature.[53] This gives an impression that silica forms part of the substrate support on which ceria has been forming a surface overlayer. This fact is elaborated latter in this paper. It is expected because the method of preparation adopted in the present study could result such a material. The absence of any other Raman features supports that silica is not forming any compound with cerium oxide under the experimental conditions employed in the present study, in agreement with the XRD measurements.

The Raman spectra of 5% and 10% $V_2O_5/CeO_2/SiO_2$ samples obtained in the range 100−1200 cm^{-1} are shown in Figures 6 (a and b) and 7, respectively. As shown in Figure 6, the 773 K calcined sample exhibits prominent Raman peaks at ∼457, ∼850, and ∼1015−1035 cm^{-1}, and few broad bands of low intensity at ∼240, ∼600, ∼720, and <100 cm^{-1}. With increasing calcination temperature from 773 to 1073 K, sharpening of the band at 457 and diminishing of few other bands can be noted. Further, at higher calcination temperatures some new bands were also observed at ∼260, ∼370, 776, 790, and 853 cm^{-1}. These bands are due to the formation of $CeVO_4$.[54] The intensity of these bands increases with increasing calcination temperature from 973 to 1073 K owing to the increase of crystallite size. No crystalline V_2O_5 features (Raman bands at ∼995, ∼702, ∼527, ∼404, ∼284, and ∼146 cm^{-1}) were found, in agreement with the XRD observations.[23] The relative intensity of the band at 600 cm^{-1} pertaining to CeO_2 decreases with increasing calcination temperature as noted for CeO_2/SiO_2 (Figure 5). The band below 100 cm^{-1} observed mainly at low calcination temperatures could be due to widening of the Rayleigh line linked to disorder. As reported in the literature,[55] the band at 1015−1035 cm^{-1} primarily corresponds to an isolated VO_4^{3-} surface species with one terminal V═O bond, the intensity of which is found to decrease with increasing calcination temperature. It is proposed that the VO_4^{3-} surface species present on the CeO_2/SiO_2 carrier will be integrated together under the influence of high-temperature calcination and interact with the ceria to form the stable $CeVO_4$ compound, thereby decreasing the amount of dispersed vanadium oxide on the surface of the support. According to literature reports, the tetrahedral VO_4^{3-}, as present in aqueous solution, has the most prominent Raman band at 827 cm^{-1}, and for solids, with isolated VO_4^{3-} units, this band lies in the range 830−855 cm^{-1}.[56] It is

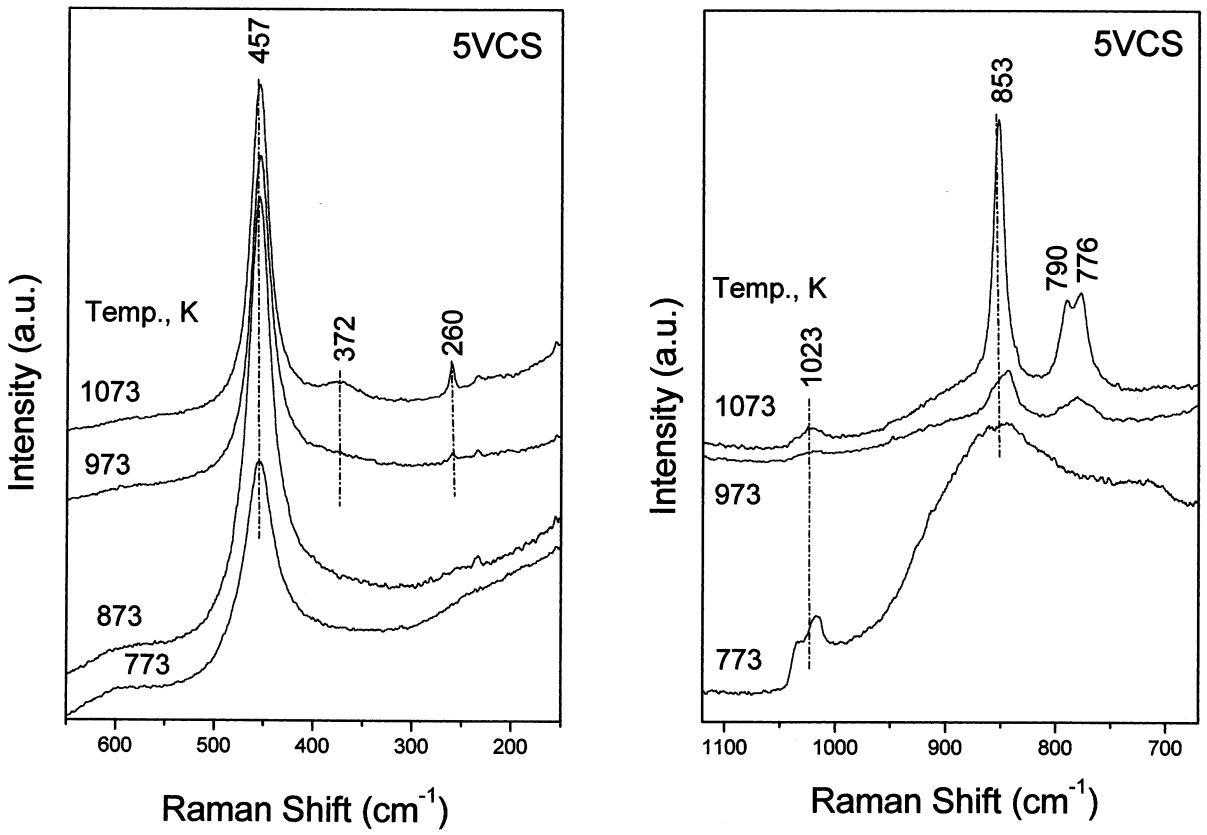

Figure 6. Laser Raman spectra of 5% $V_2O_5/CeO_2/SiO_2$ calcined at different temperatures.

associated with the breathing mode of the vanadium tetrahedron. In $CeVO_4$, vanadium ions are placed at the centers of oxygen tetrahedra with a vanadium−oxygen distance ($d_{V-O} = 1.7$ Å) similar to that of an isolated VO_4^{3-}. Therefore, the band at 853 cm^{-1} of $CeVO_4$ could be assigned to such a mode. The Raman results thus corroborate the observations made from the XRD measurements. They show the formation of $CeVO_4$ in parallel with the disappearance of dispersed vanadia and also the crystallization of CeO_2 at higher calcination temperatures. The Raman spectra pertaining to the 10% $V_2O_5/CeO_2/SiO_2$ sample, shown in Figure 7, also support these observations. In this case, the spectrum of the sample calcined at $T = 773$ K is characteristic of vanadia supported on poorly crystallized CeO_2. The spectrum of the sample calcined at 1073 K is completely different because it evidences mainly well-crystallized CeO_2 and $CeVO_4$.

The samples of CeO_2/SiO_2 and 10% $V_2O_5/CeO_2/SiO_2$ calcined at different temperatures have been investigated with XPS. The photoelectron peaks of O 1s, Si 2p, Ce 3d, and V 2p are depicted in Figures 8−11, respectively. For the purpose of better comparison, the XPS peaks of O 1s, Si 2p, and Ce 3d pertaining to the CeO_2/SiO_2 carrier and the corresponding peaks of the $V_2O_5/CeO_2/SiO_2$ sample are presented together in these figures. The corresponding binding energy (electronvolts) values and the full width at half-maximum (fwhm) values are shown in Table 2. The Ce/Si, V/Ce, and V/Si atomic ratios as determined by XPS data are shown in Figure 12. All these figures and Table 2 clearly indicate that the XPS bands and the corresponding BE values are sensitive to the calcination temperature and to the composition of the samples.[57,58]

As presented in Figure 8, the O 1s profile is, in general, more complicated due to the overlapping contribution of oxygen from ceria and silica in the case of the CeO_2/SiO_2 carrier and ceria, silica, and vanadia in the case of the $V_2O_5/CeO_2/SiO_2$ sample,

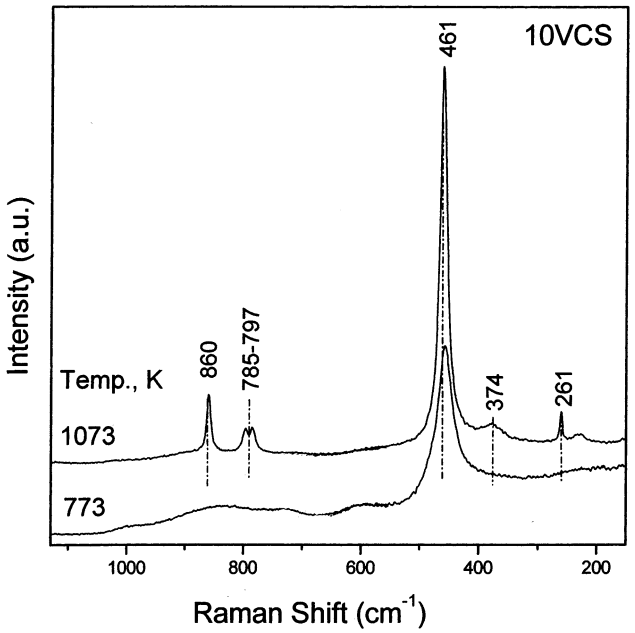

Figure 7. Laser Raman spectra of 10% $V_2O_5/CeO_2/SiO_2$ calcined at different temperatures.

respectively. The binding energy of the most intense O 1s peak (Table 2), in the case of the CeO_2/SiO_2 sample, is almost constant with increasing calcination temperature. The observed intense peak at about 530.1 eV mainly belongs to the oxygen atoms that are bound to Ce, judging from the difference in the electronegativity of the elements involved and from literature.[42,59,60] As reported in the literature,[22] the oxygen ions in pure SiO_2 and CeO_2 exhibit intense peaks at 532.7 and 528.6 eV, respectively. In the case of supported CeO_2 samples, the XPS peak was noticed at 530.3 eV.[22] Thus, the present results

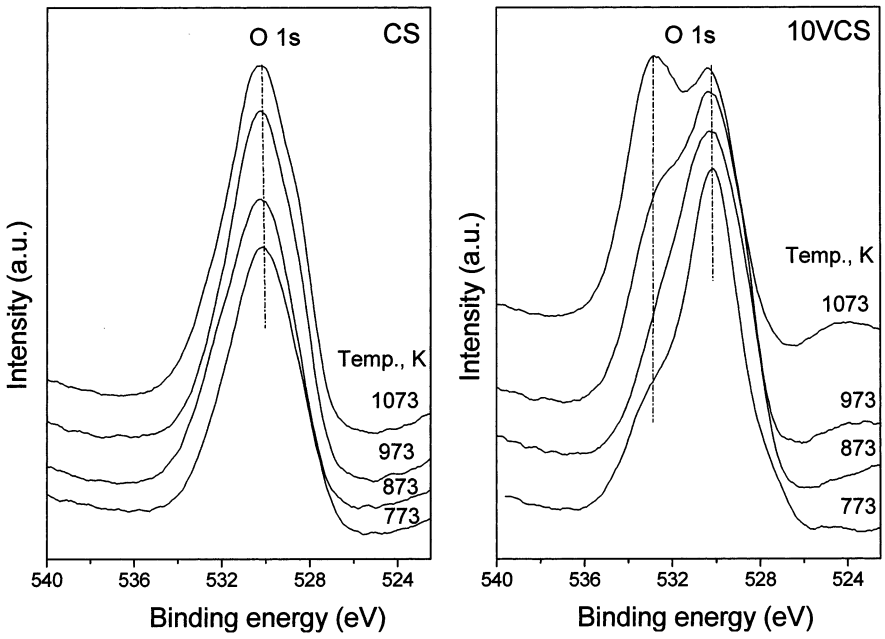

Figure 8. O 1s XPS spectra of CeO_2/SiO_2 and 10% $V_2O_5/CeO_2/SiO_2$ samples calcined at different temperatures.

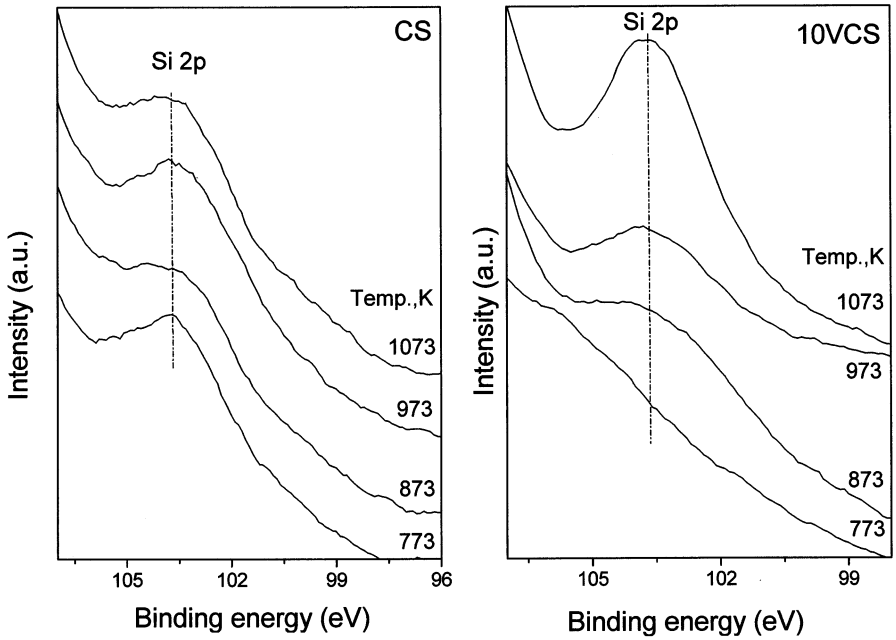

Figure 9. Si 2p XPS spectra of CeO_2/SiO_2 and 10% $V_2O_5/CeO_2/SiO_2$ samples calcined at different temperatures.

give an impression that the silica surface might be covered by ceria, as perceived from Raman study. The O 1s profile of the $V_2O_5/CeO_2/SiO_2$ sample (Figure 7b) shows much broader asymmetric peaks at 773−873 K due to overlapping contribution from CeO_2 and the dispersed V_2O_5. With increasing calcination temperature from 973 to 1073 K, bifurcation of the peak was observed, giving rise to a new peak at 532.9 eV, which may be due to the formation of $CeVO_4$ in line with XRD and Raman measurements.

As presented in Table 2, the binding energy of the Si 2p photoelectron peak ranged between 103.6 and 104.0 eV, which agrees well with the values reported in the literature.[44,61] However, the spectra (Figure 9) are very broad with less intensity, indicating that the silica surface is not easily accessible at the surface due to the presence of ceria. Further, no change in the intensity of the Si 2p core level spectra with increasing calcination temperature is observed in the case of the CeO_2/SiO_2 sample. However, in the case of $V_2O_5/CeO_2/SiO_2$ samples, an increase in the intensity of the Si 2p peak can be seen. This is mainly due to redistribution of various components in the $V_2O_5/CeO_2/SiO_2$ sample under the influence of high-temperature calcination. The strong interaction between the dispersed vanadia and the ceria to form a stable $CeVO_4$ (see XRD and Raman studies) is associated with a progressive release of the surface of SiO_2, as observed with the appearance of the intense Si 2p peak (103.7 eV) at higher calcination temperatures.

Figure 10 shows the CeO_2 3d photoelectron peaks of the CeO_2/SiO_2 and $V_2O_5/CeO_2/SiO_2$ samples calcined at different temperatures. The assignment of CeO_2 3d photoelectron peaks is ambiguous due to the complex nature of the spectra arising not only because of multiple oxidation states but also due to mixing of Ce 4f levels and O 2p states during the primary photoemission process.[22] This hybridization leads to splitting of the peaks into doublets, with each doublet showing further

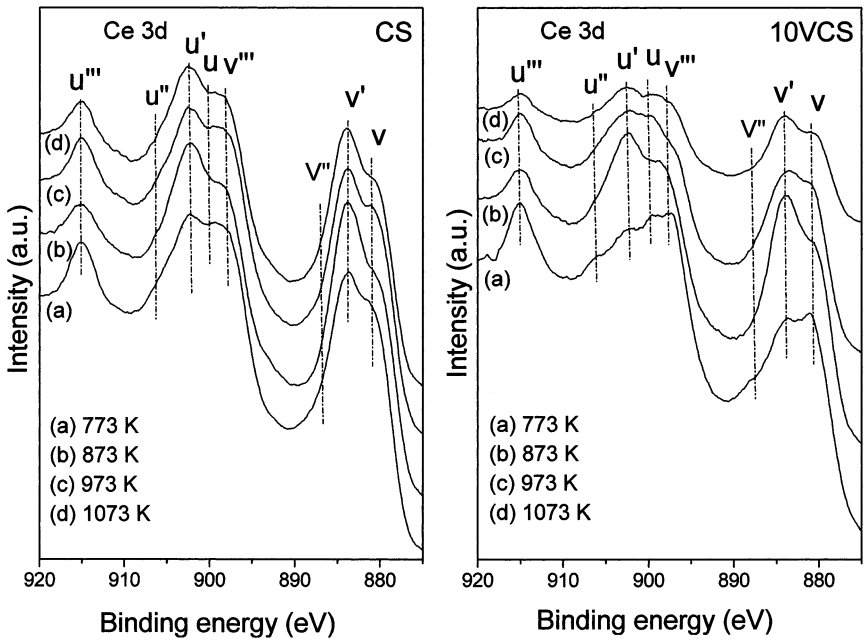

Figure 10. Ce 3d XPS spectra of CeO_2/SiO_2 and 10% $V_2O_5/CeO_2/SiO_2$ samples calcined at different temperatures.

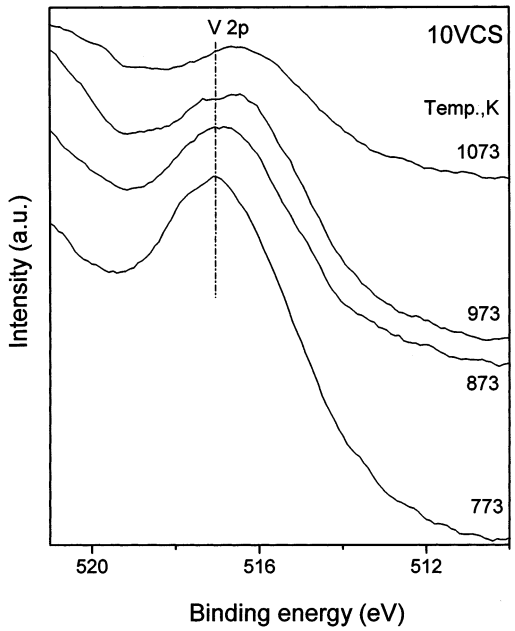

Figure 11. V 2p XPS spectra of 10% $V_2O_5/CeO_2/SiO_2$ sample calcined at different temperatures.

structure due to final-state effects. A similar complicated spectrum, as presented in Figure 10, was also reported by Stubenrauch and Vohs.[62] Using the notation of Burroughs et al.,[63] the observed peaks can be assigned for Ce(IV)O_2 as v, v″ and v‴ for Ce $3d_{5/2}$, with the corresponding Ce $3d_{3/2}$ peaks labeled as u, u″ and u‴. An additional doublet is also observed due to the presence of Ce_2O_3 (Ce^{3+}) and is assigned as v′ and u′. As seen in Figure 10a, the XPS spectrum of the pure support calcined at 773 K exhibits peaks due to the presence of both Ce^{4+} and Ce^{3+}, thus implying that cerium is present at the surface in both 4+ and 3+ oxidation states. With increasing calcination temperature the relative intensity of the u′ and v′ annotated peaks increased, indicating an increase in the surface content of Ce^{3+}. Probably the Ce^{3+} has been formed due to the reduction of CeO_2 under the conditions of ultrahigh vacuum during XPS measurements. However, the presence of Ce_2O_3 (Ce^{3+}) was not observed in the XRD patterns. In the case of the $V_2O_5/CeO_2/SiO_2$ sample, the spectrum of the sample calcined at 773 K shows two broad overlapping regions, one located between 877 and 890 eV and the second between 895 and 909 eV along with a satellite peak at 915 eV. As seen in this figure, with increasing calcination temperature, the intensity of the peaks with v′ and u′ signs increased and corresponding peaks with v‴ and u‴ notation decreased, thus indicating the stabilization of the Ce^{3+} oxidation state at higher calcination temperatures. It is obviously due to the formation of $CeVO_4$, as already noted in the discussion of the XRD and Raman measurements.

TABLE 2: XPS Core Level Electron Binding Energies (eV) and fwhm Values (eV) of the CeO_2/SiO_2 Carriers and the $V_2O_5/CeO_2/SiO_2$ Catalysts Calcined at Different Temperatures

temp	O 1s		Si $2p_{3/2}$		Ce $3d_{5/2}$		V $2p_{3/2}$	
(K)	BE	fwhm	BE	fwhm	BE	fwhm	BE	fwhm
				CeO_2/SiO_2				
773	530.1	3.7	103.7	2.9	881.7	9.8		
873	530.2	3.8	103.6	3.1	881.3	9.3		
973	530.2	3.8	103.8	3.6	881.3	9.3		
1073	530.3	3.8	103.8	3.8	881.2	9.3		
				$V_2O_5/CeO_2/SiO_2$				
773	530.1	3.2			881.1	9.8	517.1	4.2
873	530.2	4.3	104.0	3.2	880.9	9.3	516.8	4.3
973	530.3	4.9	103.9	2.8	880.8	8.8	516.6	4.4
1073	530.4	5.2	103.7	2.6	880.6	7.8	516.4	4.6

Figure 11 shows the V $2p_{3/2}$ photoelectron peak of the $V_2O_5/CeO_2/SiO_2$ sample calcined at various temperatures. A decrease in intensity and broadening of the V 2p line is observed with increasing calcination temperature. Broadening of the XPS peak can occur due to various factors including (1) the presence of more than one type of V^{5+} species with different chemical characteristics, which cannot be discerned by XPS, and (2) electron transfer between the active component and the support (metal oxide−support oxide interaction).[26,64,65] At 773 K calcination temperature the binding energy of the V $2p_{3/2}$ line is 517.1 eV. With increasing calcination temperature from 773 to 1073 K (Table 2), the binding energy of V $2p_{3/2}$ has decreased to 516.4 eV. According to the literature, the binding energy of

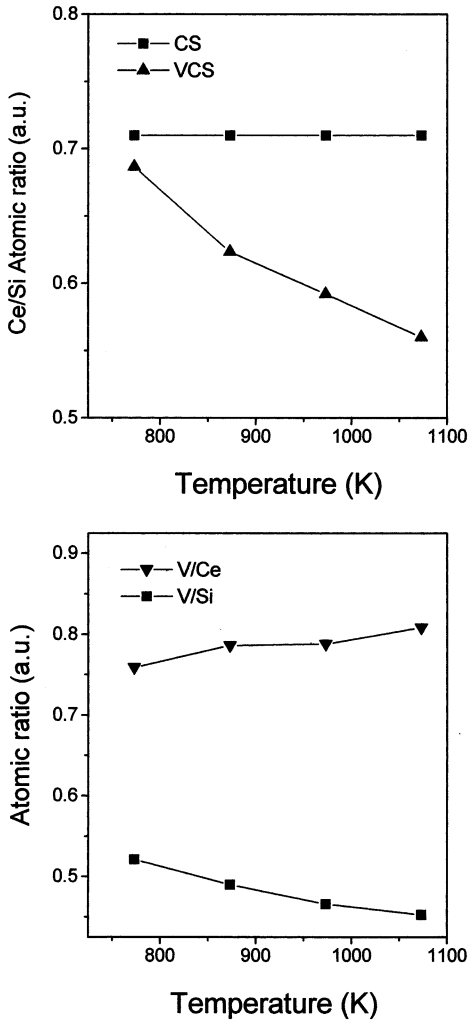

Figure 12. XPS atomic percentage ratios of CeO_2/SiO_2 and $V_2O_5/CeO_2/SiO_2$ samples at different temperatures.

V $2p_{3/2}$ reported for V_2O_5 (V^{5+} oxidation state) ranges between 517.4 and 516.4 eV; the next oxidation state, V^{4+}, represented by V_2O_4, shows values in the range 515.7−515.4 eV.[61] As presented in Table 2, there is a slight shift from 517.1 to 516.4 eV with increasing calcination, which indicates a progressive reduction of the V species at the surface under the influence of high-temperature calcination. However, most of the vanadium will be in the V(V) oxidation state due to the formation of $CeVO_4$.

The Ce/Si atomic ratios, as determined by XPS, for both CeO_2/SiO_2 and $V_2O_5/CeO_2/SiO_2$ catalysts are shown in Figure 12a. As seen in this figure, the Ce/Si atomic ratio is slightly higher for the pure support than for the vanadia-containing samples. It indicates that the CeO_2/SiO_2 surface is covered by the vanadium oxide overlayer. Another interesting observation to be noted from Figure 12a is that the Ce/Si ratio is fairly constant with increasing calcination temperature. However, the corresponding ratio in the case $V_2O_5/CeO_2/SiO_2$ sample decreased with increasing calcination temperature. This gives the impression that the CeO_2/SiO_2 carrier is thermally quite stable in the absence of vanadium oxide on its surface, which agrees with the information obtained from other techniques. However, in the case of the $V_2O_5/CeO_2/SiO_2$ sample, the decrease of the Ce/Si ratio with increasing calcination temperature is due to the formation of $CeVO_4$ on the surface of the support. The relative dispersion of vanadium oxide on the support surface was also estimated from XPS measurements of the $V_2O_5/CeO_2/SiO_2$ catalyst calcined at different temperatures and shown in Figure 12 b. The V/Ce and V/Si atomic ratios can be taken as a measure of relative dispersion of vanadium oxide on the mixed oxide surface. As observed in this figure, the V/Ce ratio increased with increasing calcination temperature, whereas the V/Si ratio decreased. It reveals clearly that most of the vanadium oxide is confined to the cerium oxide due to $CeVO_4$ compound formation. With increasing calcination temperature the $CeVO_4$ particles agglomerate into bigger particles, thereby uncovering part of the silica surface. Thus, the atomic intensity variations can be explained as due to the formation of $CeVO_4$ and the crystallization of remaining CeO_2 under the influence of high-temperature calcination.

Ease of formation and thermal stability of vanadium oxide monolayers on various supports has been related to the ratio of the charge on the support cation to the sum of radii of cation and oxide ion.[26] For SiO_2 this ratio is large and hence no surface compound formation was observed. However, for Al_2O_3 this ratio is much lower, thus accounting for the formation of mixed oxides ($AlVO_4$) at higher temperatures. Other oxides such as TiO_2, ZrO_2, and CeO_2 have intermediate values; therefore these oxides are expected to give stable vanadium oxide monolayers at typical calcination temperatures of around 773 K. It is an established fact in the literature that TiO_2 and ZrO_2 do form stable compounds with the dispersed vanadium oxide at higher calcination temperatures.[44,57] The present results also indicate the formation of a dispersed vanadium oxide layer on CeO_2 at 773 K and $CeVO_4$ at higher calcination temperatures. It should also be pointed out here that the tendency of dispersed vanadium oxide species to form surface compounds could also be related to the acid−base properties of the supports. With the acidic V_2O_5 a bidimensional vanadate is readily formed with basic MgO[26] and La_2O_3[66] at higher calcination temperatures, whereas the weak interaction with SiO_2 does not lead to compound formation. Thus, the present results suggest the formation of vanadium oxide overlayers on the ceria-covered silica surface at 773 K and a stable $CeVO_4$ compound at higher calcination temperatures. The catalytic properties of these materials for certain selective and nonselective oxidations have been evaluated and the preliminary results are found to be encouraging. Further studies are under active progress.

Conclusions

The following conclusions can be drawn from this study: (1) The CeO_2/SiO_2 composite oxide obtained by an aqueous deposition precipitation method exhibits a reasonably high specific surface area and a high thermal stability up to 1073 K. Characterization of the CeO_2/SiO_2 carrier by Raman and XPS gives an impression that the silica surface has been covered by a cerium oxide overlayer. At higher calcination temperatures it primarily consists of crystalline CeO_2 on the amorphous SiO_2 surface. (2) The CeO_2/SiO_2 composite oxide seems to be an interesting carrier for the dispersion of vanadium oxide. The impregnated vanadium oxide (5 or 10 wt %) is in a highly dispersed state on the surface of the carrier. In particular, no crystalline V_2O_5 is noted from XRD patterns and Raman spectra. The dispersed vanadium oxide selectively interacts with the ceria portion of the CeO_2/SiO_2 carrier and forms stable $CeVO_4$. Formation of this compound is highly sensitive to the calcination temperature and concentration of vanadium oxide. The dispersed vanadium oxide on the CeO_2/SiO_2 carrier also accelerates the crystallization of CeO_2. (3) The XPS electron binding energy values reveal that the $V_2O_5/CeO_2/SiO_2$ catalyst calcined at 773 K mainly contains the mixed oxide elements in the highest

oxidation states, Ce(IV), Si(IV), and V(V). With increasing calcination temperature a slight reduction of V^{5+} has been observed at the surface. However, in the case of cerium formation of Ce(III) is noted at higher calcination temperatures.

Acknowledgment. B.M.R. acknowledges visiting fellowships from Science and Technology Agency (STA), Japan, and Centre National de la Recherche Scientifique (CNRS), France. A.K. thanks the Department of Science and Technology, New Delhi, for a Research Fellowship under SERC scheme (SP/S1/H-20/98).

References and Notes

(1) Trovarelli, A. *Catal. Rev. Sci. Eng.* **1996**, *38*, 439 and references therein.
(2) Tsukama, K.; Shimada, M. *J. Mater. Sci*. **1985**, *20*, 1178.
(3) Taylor, K. C. *Catalysis Science and Technology*; Springer-Verlag: Berlin, 1984; Chapter 2.
(4) Lahaye, J.; Boehm, S.; Chambrion, P. H.; Ehrburger, P. *Combust. Flame* **1996**, *104*, 199.
(5) Matatov-Meytal, Y. I.; Sheintuch, M. *Ind. Eng. Chem. Res.* **1998**, *37*, 309.
(6) Liu, W.; Flytzani-Stephanopoulos, M. *J. Catal.* **1995**, *153*, 317.
(7) Sahibzada, M.; Steele, B. C. H.; Zheng, K.; Rudkin, R. A.; Metcalfe, I. S. *Catal. Today* **1997**, *38*, 459.
(8) Kaspar, J.; Fornasiero, P.; Graziani, M. *Catal. Today*. **1999**, *50*, 285 and references therein.
(9) Laachir, A.; Perrichon, V.; Badri, A.; Lamotte, J.; Catherine, E.; Lavalley, J. C.; El Fallah, J.; Hilarie, L.; Leonormand, F.; Quemere, E.; Sauvion, G. N.; Touret, O. *J. Chem. Soc., Faraday Trans. 1* **1991**, *87*, 1601.
(10) Kubsh, J. E.; Rieck, J. S.; Spencer, N. D. *Stud. Surf. Sci. Catal.* **1994**, *71*, 109.
(11) Sauvion, G. N.; Caillod, J.; Gourlaouen, C.; Rhone-Poulenc. Eur. Patent 0207,857, 1986.
(12) Ohata, T.; Tsuchitani, K.; Kitayuchi, S.; Nippon, S. K. Jpn. Patent 8,890,311, 1988.
(13) Ashley, N. E.; Rieck, J. S.; Grace WR and Co-Conn. U.S. Patent 484,727, 1991.
(14) Cho, B. K. *J. Catal.* **1991**, *131*, 74.
(15) Zamar, F.; Trovarelli, A.; de Leitenburg, C.; Dolcetti, G. *J. Chem. Soc., Chem. Commun.* **1995**, 965.
(16) Rao, G. R.; Fornasiero, P.; Di Monte, R.; Kaspar, J.; Vlaic, G.; Balducci, G.; Meriani, S.; Gubitosa, G.; Cremona, A.; Graziani, M. *J. Catal.* **1996**, *162*, 1.
(17) Pijolat, M.; Prin, M.; Soustelle, M.; Tourer, O.; Nortier, P. *J. Chem. Soc., Faraday Trans.* **1995**, *91*, 3941.
(18) Fornasiero, P.; Di Monte, R.; Rao, G. R.; Kaspar, J.; Meriani, S.; Trovarelli, A.; Graziani, M. *J. Catal.* **1995**, *151*, 168.
(19) Zamar, F.; Trovarelli, A.; de Leitenburg, C.; Dolcetti, G. *Stud. Surf. Sci. Catal.* **1996**, *101*, 1283.
(20) Miki, T.; Ogawa, T.; Haneda, M.; Kakuta, N.; Ueno, A.; Tateishi, S.; Matsura, S.; Sato, M. *J. Phys. Chem.* **1990**, *94*, 6464.
(21) Logan, A. D.; Shelef, M. *J. Mater. Res*. **1994**, *9*, 468.
(22) Bensalem, A.; Bozon-Verduraz, F.; Delamar, M.; Bugli, G. *Appl. Catal. A: General* **1995**, *121*, 81.
(23) Jih-Mirn Jehng. *J. Phys. Chem. B* **1998**, *102*, 5816.
(24) Védrine, J. C., Ed. Eurocat Oxide. *Catal. Today* **1994**, *20*, 1.
(25) Gellings, P. J. In *Catalysis*; Bond, G. C., Webb, G., Eds.; The Royal Society of Chemistry: London, 1985; Vol. 7, p 105.
(26) Bond, G. C.; Tahir, S. F. *Appl. Catal.* **1991**, *71*, 1 and references therein.
(27) Deo, G.; Wachs, I. E.; Haber, J. *Crit. Rev. Surf. Chem.* **1994**, *4*, 141.
(28) Bosch, H.; Janssen, F. *Catal. Today* **1988**, *2*, 369.
(29) Roozeboom, F.; Mittelmeijer-Hazeleger, M. C.; Moulijn, J. A.; Medema, J.; de Beer, V. H.; Gellings, P. J. *J. Phys. Chem.* **1980**, *84*, 2783.
(30) Reddy, B. M.; Reddy, E. P.; Srinivas, S. T.; Mastikin, V. M.; Nosov, A. V.; Lapina, O. B. *J. Phys. Chem*. **1992**, *96*, 7076.
(31) Eon, J. G.; Olier, R.; Volta, J. C. *J. Catal.* **1994**, *145*, 318.
(32) Kung, H. H.; Kung, M. C. *Appl. Catal. A: General* **1997**, *157*, 105.
(33) Khodakov, A.; Olthof, B.; Bell, A. T.; Iglesia, E. *J. Catal.* **1999**, *181*, 205.
(34) Zhao, Z.; Yamada, Y.; Teng, Y.; Ueda, A.; Nakagawa, K.; Kobayashi, T. *J. Catal.* **2000**, *190*, 215.
(35) Concepción, P.; Reddy, B. M.; Knözinger, H. *Phys. Chem. Chem. Phys.* **1999**, *1*, 3031.
(36) Baiker, A.; Dollenmeier, P.; Glinski, M.; Reller, A. *Appl. Catal.* **1997**, *35*, 351.
(37) Oyama, S. T.; Went, G. T.; Lewis, K. B.; Bell, A. T.; Somorjai, G. A. *J. Phys. Chem.* **1989**, *93*, 6786.
(38) Reddy, B. M.; Chowdhury, B.; Reddy, E. P.; Fernández, A. *Langmuir* **2001**, *17*, 1132
(39) Véjux, A.; Courtine, P. *J. Solid State Chem.* **1978**, *23*, 93.
(40) Deo, G.; Wachs, I. E. *J. Catal*. **1991**, *129*, 307.
(41) Klug, H. P.; Alexander, L. E. *X-ray Diffraction Procedures for Polycrystalline and amorphous materials*, 2nd ed.; John Wiley and Sons: New York, 1974.
(42) Briggs, D., Seah, M. P., Eds. Auger and X−Ray Photoelectron Spectroscopy. *Practical Surface Analysis*, 2nd ed.; Wiley: New York, 1990; Vol. 1
(43) Wagner, C. D.; Riggs, W. M.; Davis, L. E.; Moulder, J. F. In *Handbook of X-ray Photoelectron Spectroscopy*; Muilenberg, G. E., Ed.; Perkin-Elmer Corp.: CITY, MN, 1978.
(44) Reddy, B. M.; Ganesh, I.; Reddy, E. P. *J. Phys. Chem. B* **1997**, *101*, 1769.
(45) Reddy, B. M.; Manohar, B.; Reddy, E. P. *Langmuir* **1993**, *9*, 1781.
(46) Colon, G.; Valdivieso, F.; Pijolat, M.; Baker, R. T.; Calvino, J. J.; Bernal, S. *Catal. Today* 1**999**, *50*, 271.
(47) Rynkowski, J.; Farbotko, J.; Touroude, R.; Hilaire, L. *Appl. Catal. A: General* **2000**, *203*, 335.
(48) Wachs, I. E.; Hardcastle, F. D.; Chan, S. S. *Spectroscopy* **1986**, *1*, 30.
(49) Lin, X.-M.; Li, L.-P.; Li, G.-S.; Su, W.-H. *Mater. Chem. Phys*. **2001**, *69*, 236.
(50) Spanier, J. E.; Robinson, R. D.; Zhang, F.; Chan, S.-W.; Herman, I. P. *Phys. Rev. B* **2001**, *64*, 245407.
(51) Weber, W. H.; Hass, K. C.; McBride, J. R. *Phys. Rev. B* **1993**, *48*, 178.
(52) McBride, J. R.; Hass, K. C.; Poindexter, B. D.; Weber, W. H. *J. Appl. Phys*. 1**994**, *76*, 2435.
(53) Wachs, I. E.; Deo, G. *J. Phys. Chem.* **1991**, *95*, 5889.
(54) Hirata, T.; Watanabe, A. *J. Solid State Chem*. **2001**, *158*, 254.
(55) Eckert, H.; Wach, I. E. *J. Phys. Chem*. **1989**, *93*, 6796.
(56) Griffith, W. P.; Lesniak, P. J. B. *J. Chem Soc. A* **1969**, 1066.
(57) Reddy, B. M.; Chowdhary, B.; Ganesh, I.; Reddy, E. P.; Rojas, T. C.; Fernández, A. *J. Phys. Chem. B* **1998**, *102*, 10176.
(58) Galan-Fereres, M.; Mariscal, R.; Alemany, L. J.; Fierro, J. L. G.; Anderson, J. A. *J. Chem. Soc., Faraday Trans*. **1994**, *90*, 3711.
(59) Imamura, I.; Ishida, S.; Taramoto, H.; Saito, Y. *J. Chem. Soc., Faraday Trans.* **1993**, *89*, 757.
(60) Sawatzky, G. A.; Post, D. *Phys. Rev.* **1979**, *B 20*, 1546.
(61) Bukhtiyarov, V. I. *Catal. Today* **2000**, *56*, 403.
(62) Stubenrauch, J.; Vohs, J. M. *J. Catal*. **1996**, *159*, 50.
(63) Burroughs, A.; Hamnett, A.; Orchard, A. F.; Thornton, G. *J. Chem. Soc., Dalton Trans*. **1976**, *1*, 1686.
(64) Nag, N. K.; Massoth, F. E. *J. Catal*. **1990**, *124*, 127.
(65) Nogier, J. Ph.; Delmer, M. *Catal Today* **1994**, *20*, 109.
(66) Reddy, B. M.; Sreekanth, P. M.; Reddy, E. P.; Yamada, Y.; Qiang, X.;Kobayashi, T. *J. Phys. Chem. B* **2002**, *106*, 5695.